POLITECNICO DI TORINO
Repository ISTITUZIONALE

The new CCSDS standard for low-complexity lossless and near-lossless multispectral and hyperspectral image compression

Original
The new CCSDS standard for low-complexity lossless and near-lossless multispectral and hyperspectral image compression / Kiely, Aaron; Klimesh, Matthew; Blanes, Ian; Ligo, Jonathan; Magli, Enrico; Aranki, Nazeeh; Burl, Michael; Camarero, Roberto; Cheng, Michael; Dolinar, Sam; Dolman, David; Flesch, Greg; Ghassemi, Hamid; Gilbert, Martin; Hernandez-Cabronero, Miguel; Keymeulen, Didier; Le, Martin; Luong, Huy; Mcguinness, Christopher; Moury, Gilles; Pham, Thang; Plintovic, Martin; Sala, Frederic; Santos, Lucana; Schaar, Alan; Serra-Sagrista, Joan; Shin, Simon; Sundlie, Brenton; Valsesia, Diego; Vitulli, Raffaele; Wong, Englin; Wu, William; Xie, Hua; Zhou, Hanying. - (2018), pp. 1-7. ((Intervento presentato al convegno 2018 Onboard Payload Data Compression Workshop tenutosi a Matera, Italy nel Sept. 2018.

Availability:
This version is available at: 11583/2728880 since: 2019-04-12T13:27:58Z

Publisher:
ESA

Published
DOI:

Terms of use:
openAccess

This article is made available under terms and conditions as specified in the corresponding bibliographic description in the repository

Publisher copyright

(Article begins on next page)

04 August 2020

THE NEW CCSDS STANDARD FOR LOW-COMPLEXITY LOSSLESS AND NEAR-LOSSLESS MULTISPECTRAL AND HYPERSPECTRAL IMAGE COMPRESSION

Aaron Kiely[1], Matthew Klimesh[1], Ian Blanes[2], Jonathan Ligo[3], Enrico Magli[4], Nazeeh Aranki[1], Michael Burl[1], Roberto Camarero[5], Michael Cheng[1], Sam Dolinar[1], David Dolman[6], Greg Flesch[1], Hamid Ghassemi[1], Martin Gilbert[1], Miguel Hernández-Cabronero[2], Didier Keymeulen[1], Martin Le[1], Huy Luong[1], Christopher McGuinness[7], Gilles Moury[5], Thang Pham[1], Martin Plintovic[8], Frederic Sala[3], Lucana Santos[9], Alan Schaar[10], Joan Serra-Sagristà[2], Simon Shin[1], Brenton Sundlie[7], Diego Valsesia[4], Raffaele Vitulli[9], Englin Wong[11], William Wu[3], Hua Xie[1], Hanying Zhou[1]

[1]*Jet Propulsion Laboratory, California Institute of Technology, 4800 Oak Grove Drive, Pasadena, CA 91109 USA, Email: {Aaron.B.Kiely, Matthew.A.Klimesh}@jpl.caltech.edu*
[2]*Dept. of Information and Communications Engineering, Universitat Autònoma de Barcelona, Campus UAB, 08193 Cerdanyola del Vallès (Barcelona), Spain, Email: {ian.blanes, joan.serra}@uab.cat, mhernandez@deic.uab.cat*
[3]*Work conducted at Jet Propulsion Laboratory, California Institute of Technology*
[4]*Politecnico di Torino, Dept. of Electronics and Telecommunications, C.so Duca degli Abruzzi, 24,10129 Torino - Italy, Email: {enrico.magli, diego.valsesia}@polito.it*
[5]*Centre National d'Études Spatiales, On-Board Data Systems Office (DSO/TB/ET), 18 avenue Edouard Belin 31401 Toulouse Cedex 9, France, Email: {Roberto.Camarero, Gilles.Moury}@cnes.fr*
[6]*Alpha Data Parallel Systems Ltd., 4 West Silvermills Lane, Edinburgh, EH3 5BD, Scotland, UK, Email: david.dolman@alpha-data.com*
[7]*University of Dayton Research Institute, 2275 Rustic View Dr., Beavercreek, OH 45431 USA, Email: {Christopher.McGuinness, Brenton.Sundlie}@udri.udayton.edu*
[8]*Airbus Defence & Space GmbH, Claude-Dornier-Str., 88090 Immenstaad, Germany, Email: martin.plintovic@airbus.com*
[9]*European Space Agency, ESA/ESTEC, Keplerlaan 1, 2201AZ Noordwijk (NL), Email: {Raffaele.Vitulli, Lucana.Santos}@esa.int*
[10]*Air Force Life Cycle Management Center, 2530 Loop Rd W., WPAFB, OH 45433, USA, Email: alan.schaar.ctr@us.af.mil*
[11]*NASA Goddard Space Flight Center, B19 RM S026, 8800 greenbelt Rd., Greenbelt, MD 20771, USA, Email: mark.wong@nasa.gov*

ABSTRACT

This paper describes the emerging Issue 2 of the CCSDS-123.0-B standard for low-complexity compression of multispectral and hyperspectral imagery, focusing on its new features and capabilities. Most significantly, this new issue incorporates a closed-loop quantization scheme to provide near-lossless compression capability while still supporting lossless compression, and introduces a new entropy coding option that provides better compression of low-entropy data.

1. INTRODUCTION

In 2012, Issue 1 of the CCSDS-123.0-B standard for lossless compression of multispectral and hyperspectral images was published [1].

Because of the significant data volume reduction often needed to meet spacecraft downlink limitations, lossy compression is becoming increasingly used in space applications. With this motivation, the Consultative Committee for Space Data Systems (CCSDS) Multispectral and Hyperspectral Data Compression (MHDC) working group has been developing Issue 2 of CCSDS-123.0-B, extending the standard's capabilities to provide low-complexity near-lossless compression while still supporting lossless compression. In this context, "near-lossless" refers to the ability to perform compression in a way that limits the maximum error in the reconstructed image to a user-specified bound.

This paper describes Issue 2, focusing on its new features and capabilities. A companion paper [2] provides an in-depth analysis of parameter selection to optimize performance.

We note that while the MHDC working group has reached consensus on the new specification, the standard has not yet been published and so there is some possibility that, as a result of the CCSDS review process, details could change from the description provided here.

We assume that readers are familiar with [1] and the notation introduced therein. Following the convention

of the standard, here data samples and associated quantities may be identified via three coordinate indices x, y, z, (e.g., $s_{z,y,x}$) or the pair of indices z, t, (e.g., $s_z(t)$), where the value of t corresponds to the index of the sample within spectral band z when samples in the band are arranged in raster-scan order.

The most significant new feature of Issue 2 is the incorporation of a closed-loop scalar quantizer in the compressor's prediction stage to provide near-lossless compression. Users can control quantizer step size by specifying an *absolute error limit*, so that samples can be reconstructed with a user-specified bound on reconstruction error, and/or a *relative error limit*, so that samples predicted to have smaller magnitude can be reconstructed with lower error. Quantizer fidelity settings can vary from band to band and can be updated periodically within the image.

The predictor cannot in general utilize the exact values of the original data samples because these values will not be available to the decompressor at the time of reconstruction when compression is not lossless. Instead, prediction calculations are performed using a *sample representative* in place of each original sample value. For some images, the obvious choice of setting the sample representative equal to the center of the quantization bin for the sample does not give the best compression performance; user-specified parameters that control the calculation of sample representatives allow a user to exploit this fact to improve compression performance in some cases.

A new entropy coding option provides better compression of low-entropy data, which become increasingly prevalent as quantization step size increases. This *hybrid* entropy coder includes codes equivalent to those used by the sample-adaptive encoder defined in Issue 1, but augmented with an additional 16 variable-to-variable length "low-entropy" codes. A single output codeword from a low-entropy code may encode multiple samples, which allows lower compressed data rates.

Issue 2 supports high-dynamic-range instruments, allowing up to 32-bit signed and unsigned integer samples, an increase from the 16-bit limit under Issue 1.

The compressed image syntax is extended to support the inclusion of optional *supplementary information tables*, which can provide ancillary image or instrument information to the end user, e.g., to identify malfunctioning elements in a detector array or the wavelength associated with each spectral band. Each such table is a one-dimensional (one element for each band z) or two-dimensional (one element for each (z, x)

pair, or each (y, x) pair) table of floating-point, signed integer, or unsigned integer values.

Section 2 gives a brief overview of the compressor. Key changes to the prediction stage and the entropy coder are described in Sections 3 and 4 respectively.

2. OVERVIEW

The CCSDS-123.0-B-1 (Issue 1) standard[1] is based on the Fast Lossless (FL) compressor, a low-complexity lossless compression algorithm designed to exploit spectral dependencies and the three-dimensional structure of multispectral and hyperspectral images [1][3][4].

Issue 2 is based largely on the FL Extended (FLEX) compressor, which extends FL to provide adjustable near-lossless compression in addition to lossless compression [5]. FLEX inherits many of the desirable features of the FL compressor, such as low computational complexity, single-pass compression and decompression, and automatic adaptation to the source image data.

Issue 2 incorporates an improvement of FLEX's hybrid entropy coder, and adds features such as relative error limits, periodic error limit updating (see Section 3.1), and narrow local sums (see Section 3.3).

In July 2018, the FLEX compressor began use onboard the International Space Station as part of NASA's ECOsystem Spaceborne Thermal Radiometer Experiment on Space Station (ECOSTRESS) instrument. This compressor implementation is in a Virtex 5 FX130T operating at 25 MHz with 4×512 MB SDRAM, out of which 3 MBytes are used as scratchpad memory, and 256 Gbytes mass storage with a data read throughput of 135 Mbits/sec [5]. The mass storage is used only for raw uncompressed data acquired from the focal plane array. The compressor achieves throughput of 1 Msample/sec, with a typical lossless data compression ratio of 2.3:1 on the 16-bit samples produced by the instrument. A higher throughput implementation of FLEX is presented in [6].

Fig. 1 depicts the components of the Issue 2 compressor, consisting of a predictor followed by an encoder.

---

[1] In CCSDS nomenclature, the "-1" at the end of "CCSDS-123.0-B-1" indicates Issue 1.
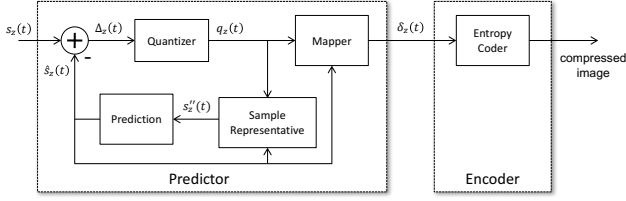
Figure 1. Compressor Schematic

The predictor, described in Section 3, uses an adaptive linear prediction method to predict the value of each image sample based on the values of nearby samples in a small three-dimensional neighborhood. Prediction can be performed causally in a single pass through the image. The prediction residual is quantized, and the quantizer output is mapped to an unsigned integer *mapped quantizer index* $\delta_z(t)$, similar to the calculation of mapped prediction residuals in Issue 1. This mapping is invertible, so that the decompressor can exactly reconstruct the quantizer index. These mapped quantizer indices make up the output of the predictor.

The encoder losslessly encodes the sequence of mapped quantizer indices. Section 4 describes the new entropy coding option, which combines a family of codes, equivalent to the length-limited Golomb-Power-of-2 (GPO2) codes [7] used by the sample-adaptive coding option of the Issue 1 standard, along with 16 new variable-to-variable length codes designed to provide more effective compression of low-entropy samples. This *hybrid* coding approach adaptively switches between these two coding methods on a sample-by-sample basis.

All features available in Issue 1 have been retained and Issue 2 has been designed to be backward compatible with Issue 1. Thus, compressed images produced by a compressor that is compliant with Issue 1 will also be compliant with Issue 2.

Note that features added in Issue 2 are not limited to those that provide near-lossless compression capabilities. Thus, e.g., a losslessly compressed image that is compliant with Issue 2 might not be decompressible with a decompressor that is compliant with Issue 1. On that note, even when compression is lossless, the use of the new entropy coder and sample representative calculation can sometimes provide improved compression performance over Issue 1, as illustrated in Tab. 1.

3. PREDICTOR

The predictor differs from that of Issue 1 in two major respects. First, each prediction residual $\Delta_z(t)$ is quantized using a uniform quantizer with step size determined by user-specified fidelity parameters as described below in Section 3.1. Second, the predictor

cannot utilize the original sample values $s_z(t)$, because these values will not be available to the decompressor at the time of reconstruction. Instead, prediction calculations are performed using a *sample representative* $s_z''(t)$ in place of each original sample value $s_z(t)$, as described in Section 3.2.

A new optional modification to the prediction calculation, intended to reduce prediction complexity, is discussed in Section 3.3.

3.1. Quantization

User-specified *absolute* and/or *relative error limit* values control the *maximum error* value $m_z(t)$ for each sample. The prediction residual,

$$\Delta_z(t) = s_z(t) - \hat{s}_z(t) \qquad (1)$$

Table 1. Lossless compression data rates for Issue 1 (using the sample-adaptive entropy coder) and Issue 2 (using the hybrid entropy coder and selecting good sample representative parameter values)

Instrument	# bands	Data rate (bits/sample)		Δrate (bits/ sample)
		Issue 1	Issue 2	
IASI	8461	4.75	4.75	0.00
AIRS	1501	4.30	4.22	0.08
CRISM FRT	545	5.06	4.89	0.17
CRISM HRL	545	4.57	4.40	0.17
CRISM MSP	74	2.55	2.51	0.04
AVIRIS-NG rad1	432	6.91	6.60	0.31
AVIRIS-NG rad2	432	5.36	5.06	0.31
AVIRIS-NG raw	432	5.12	4.86	0.26
M3 target	260	3.09	2.96	0.13
M3 global	86	2.14	2.17	-0.02
M3 rad1	85	6.60	6.55	0.05
M3 rad2	85	2.21	2.17	0.04
Hyperion flatfield	242	3.97	3.91	0.06
Hyperion raw	242	4.31	4.20	0.12
SFSI radiance	240	2.96	2.87	0.09
SFSI raw	240	4.67	4.48	0.19
AVIRIS_16 rad	224	3.74	3.70	0.04
AVIRIS_16 raw	224	5.98	5.95	0.02
AVIRIS_12 raw	224	2.68	2.62	0.06
HICO_128	128	5.10	5.00	0.11
HICO_87	87	4.29	4.27	0.01
CASI radiance	72	7.80	7.77	0.02
CASI raw	72	4.99	4.97	0.03
MODIS night	17	4.73	4.72	0.01
MODIS day	14	5.77	5.62	0.15
MODIS 500	5	7.20	7.17	0.03
MODIS 250	2	6.48	6.48	0.01
MSG	11	3.39	3.35	0.04
LANDSAT	6	3.37	3.35	0.02
PLEIADES	4	7.11	7.10	0.01
VEGETATION	4	5.15	5.14	0.01
SPOT	3	4.53	4.52	0.00

is quantized by a uniform quantizer centered at $\hat{s}_z(t)$ and having step size $2m_z(t) + 1$, which guarantees that the sample can be reconstructed with at most $m_z(t)$ units of error.

Users can choose to use lossless compression, which sets $m_z(t) = 0$ for all z and t. Alternatively, users can control the maximum error value by specifying an *absolute error limit* a_z for each z, a *relative error limit* r_z for each z, or both.

When only absolute error limits are used, the maximum error is computed as

$$m_z(t) = a_z \qquad (2)$$

for all z and t; when only relative error limits are used,

$$m_z(t) = \left\lfloor \frac{r_z |\hat{s}_z(t)|}{2^D} \right\rfloor \qquad (3)$$

for all z and t, so that samples predicted to have smaller magnitude can be reconstructed with higher fidelity; and when both absolute and relative error limits are used,

$$m_z(t) = \min\left(a_z, \left\lfloor \frac{r_z |\hat{s}_z(t)|}{2^D} \right\rfloor \right) \qquad (4)$$

for all z and t.

By varying the values of a_z and/or r_z from band to band, bands with higher science value can be preserved with higher fidelity (or losslessly) while reducing the data volume used to encode bands with lower science value.

Error limit values may be fixed for an entire image, or the user may choose to use *periodic error limit updating*, in which case new error limit values are periodically encoded in the compressed bitstream. This capability could be used, for example, to provide higher fidelity data for regions of an image that are expected to contain features of interest, or to adaptively adjust fidelity parameters to meet a downlink rate constraint. Note that the standard does not specify a particular method for selecting error limit values to meet such a constraint, because error limit values are encoded in the bitstream, and so the decompressor does not need to know how these values were selected.

3.2. Sample Representatives

Because compression may not be lossless, the original sample values may not available to the decompressor. Consequently, a *sample representative* $s_z''(t)$ is used in

place of the original sample value for the purpose of calculating subsequent predictions.

At the decompressor, reconstructing each sample to equal the center of the quantizer bin, $s_z'(t)$, will minimize the maximum reconstruction error. However, this choice may not minimize other distortion metrics such as mean squared error.

Similarly, selecting the sample representative $s_z''(t)$ to be equal to $s_z'(t)$, which is the traditional predictive compression approach, does not always optimize compression performance, even when compression is lossless.

For this reason, user-specified parameters ϕ_z, ψ_z, Θ are used to control the calculation of sample representatives. The sample representative $s_z''(t)$ is an integer approximation to

$$\frac{\phi_z}{2^\Theta} \hat{s}_z(t) + \left(1 - \frac{\phi_z}{2^\Theta} \right) \left(s_z'(t) - \frac{\psi_z}{2^\Theta} \operatorname{sgn}[q_z(t)] m_z(t) \right) \qquad (5)$$

as illustrated in Fig. 2. The sample representative always lies in the range from quantizer bin center $s_z'(t)$ to the predicted sample value $\hat{s}_z(t)$; the values of ϕ_z, ψ_z, Θ control the compromise between these two limits. Setting $\phi_z = \psi_z = 0$ causes the sample representative to be equal to $s_z'(t)$, and larger values of these parameters yield sample representative values closer to $\hat{s}_z(t)$. Note that the sample representative may be outside of the quantizer bin containing $s_z'(t)$.
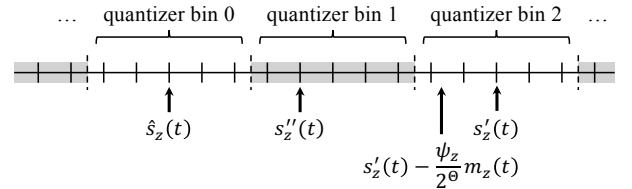
Figure 2. Possible sample representative calculation quantities, illustrated here for $m_z(t) = 2$, $q_z(t) = 2$, and nonzero values of ϕ_z and ψ_z.

Experiments suggest that using nonzero values for sample representative parameters tends to provide more benefit when spectral bands are more closely spaced in wavelength and when image noise level is higher.

Using nonzero values for ϕ_z and ψ_z can yield lower compressed data rate due to improved prediction accuracy. Less obvious is that this may also provide improved reconstructed image quality in some bands under lossy compression. As an example, Fig. 3 shows histograms of reconstruction error in one band of a test

image compressed with absolute error limit $a_z = 5$, using two different choices for sample representative parameters. The maximum error in this band is the same under both approaches, but here MSE distortion in this band is improved by using nonzero values of ϕ_z and ψ_z.
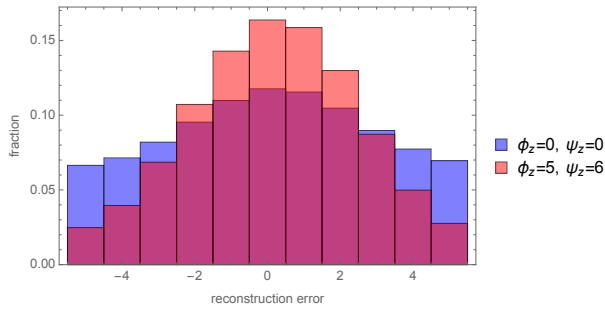

Figure 3. Histograms of reconstruction error for a single band of a test image for two different choices of sample representative parameters; here $\Theta = 4$.

3.3. Narrow Local Sums

Issue 2 introduces a new option to use *narrow* local sums of neighboring sample representatives in the prediction calculation. When combined with reduced prediction mode, the use of narrow local sums eliminates the dependency on sample representative $s''_{z,y,x-1}$ when performing the prediction calculation for neighboring sample $\hat{s}_{z,y,x}$. Eliminating this dependency may facilitate pipelining in a hardware implementation, though generally at the expense of somewhat reduced compression effectiveness [2].

3.4. Weight Exponent Offsets

Issue 2 introduces an additional *weight exponent offset* term in the exponent of each prediction weight update equation. These user-specified quantities are intended to better accommodate band-to-band variations in signal energy in the input image.

4. ENTROPY CODING

The mapped quantizer indices output from the prediction stage are losslessly encoded by the encoder. Issue 2 retains the two entropy coding options defined in Issue 1: the *sample-adaptive* encoder based on length-limited GPO2 codes, and the *block-adaptive* encoder based on the Rice coder as formalized in CCSDS-121.0-B-2 [8].

Issue 2 also introduces a new *hybrid* entropy coding option, which provides better compression of low-entropy data than achieved by the two legacy coding options. Such low-entropy data becomes more prevalent with the introduction of near-lossless compression capabilities. The remainder of this section describes the hybrid encoder.

The hybrid encoder uses adaptive code selection statistics, described in Section 4.1, that are similar to those used by the sample-adaptive coder. It uses codes equivalent to those used by the sample-adaptive encoder, but augmented with an additional 16 variable-to-variable length "low-entropy" codes described in Section 4.2.

An interesting feature of the hybrid entropy coder is that it is designed so that decoding proceeds in reverse order. This permits a simpler and more memory-efficient encoder than FLEX's original hybrid entropy coder, which was based on an interleaved entropy coding approach [9][10].

4.1. Code Selection Statistics

For each band z, the hybrid encoder maintains a *high-resolution accumulator* $\tilde{\Sigma}_z(t)$ and a *counter* $\Gamma(t)$. With each new mapped quantizer index $\delta_z(t)$, the high-resolution accumulator is incremented by $4\delta_z(t)$; the counter is incremented by one when t is incremented. Both the counter and accumulator are rescaled periodically at an interval controlled by a user-specified parameter. These code selection statistics are similar to the corresponding ones for the sample-adaptive encoder, except that the accumulator for the hybrid coder has higher resolution, and updates to code selection statistics are performed *before* encoding $\delta_z(t)$, because decoding proceeds in reverse order.

The ratio $\tilde{\Sigma}_z(t)/\Gamma(t)$ represents a scaled estimate of the mean mapped quantizer index for band z. This ratio determines the coding method used to encode $\delta_z(t)$. If this ratio exceeds a fixed threshold, then $\delta_z(t)$ is said to correspond to a "high-entropy" sample, otherwise $\delta_z(t)$ is said to correspond to a "low-entropy" sample. For both high-entropy and low-entropy samples, this ratio also determines the specific code used to encode $\delta_z(t)$.

4.2. Encoding

Each high-entropy mapped quantizer index is encoded using a variable-length binary codeword from a family of codes. Each code in the family is equivalent to a length-limited GPO2 code, but with the output bits arranged in a different order so that the code is suffix-free.

The encoding of each low-entropy mapped quantizer index makes use of one of 16 variable-to-variable length codes. A single output codeword from a low-entropy code may encode multiple mapped quantizer indices, which allows lower compressed data rates than can be achieved by the high-entropy codes. Each high-entropy mapped quantizer index immediately produces an output codeword that is written to the compressed bitstream, while each low-entropy code waits until

enough data has arrived to determine the next output codeword.

By decoding the compressed image body in reverse order, the decoder can accommodate the varying latency between the arrival of a low-entropy mapped quantizer index and its ultimate encoding. This is possible because (1) the output codewords from the high- and low-entropy codes are suffix-free rather than prefix-free, (2) the compressed image ends with a "tail" that encodes the final state of each low-entropy code and the final high-resolution accumulator value for each band, and (3) immediately prior to each rescaling of the high-resolution accumulator, the high-resolution accumulator's least significant bit is output so that the decoder can invert this rescaling operation.

Each of the 16 low-entropy codes is a nonbinary-input, binary-output, variable-to-variable length code that defines a mapping from an exhaustive prefix-free set of variable length *input codewords* over an input symbol alphabet that varies from code to code, onto an exhaustive suffix-free set of variable length binary *output codewords*.

Associated with each low-entropy code is an integer input symbol limit L_i, between 0 and 12 inclusive. We can think of L_i as distinguishing between "likely" values ($\delta_z(t) \leq L_i$) and "unlikely" values ($\delta_z(t) > L_i$).

If $\delta_z(t)$ is a likely value for the code ($\delta_z(t) \leq L_i$), then the component code encodes the value of $\delta_z(t)$. Otherwise, it encodes an "escape" symbol, indicating that $\delta_z(t)$ was an unlikely symbol ($\delta_z(t) > L_i$) and the nonnegative residual value $\delta_z(t) - L_i - 1$ is encoded, using a code that is equivalent to a length-limited unary codeword, immediately preceding the output codeword from the low-entropy code. Since escape symbols occur with low probability, the efficiency with which these residual values are encoded has only a small impact on overall coding effectiveness.

Input symbols assigned to a given low-entropy code are collected until a complete input codeword is formed for that code. The component codes are designed so that an escape symbol always causes the completion of an input codeword, and so at most one residual value will accompany any output codeword from a low-entropy code.

The input symbol limit L_i limits the size of the input alphabet in the low-entropy codes, by treating all unlikely symbols in the same way. This allows us to reduce the number of codewords in a component code. Tab. 2 shows the sizes of the component codes used.

Table 2. Low-entropy code sizes

Code Index	Input Symbol Limit	Number of Codewords	Max. Input Length	Max. Output Length (bits)
0	12	105	3	13
1	10	144	3	13
2	8	118	3	12
3	6	120	4	13
4	6	92	4	13
5	4	116	6	15
6	4	101	6	15
7	4	81	5	18
8	2	88	12	16
9	2	106	12	17
10	2	103	12	18
11	2	127	16	20
12	2	109	27	21
13	2	145	46	18
14	2	256	85	17
15	0	257	256	9

6. REFERENCES

[1] *Lossless Multispectral & Hyperspectral Image Compression*. Recommendation for Space Data System Standards, CCSDS 123.0-B-1. Blue Book. Issue 1. Washington, D.C.: CCSDS, May 2012.

[2]   I. Blanes, A. Kiely, J. Serra-Sagristà, M. Hernández-Cabronero, "Performance Impact of Parameter Tuning on the Emerging CCSDS 123.0-B-2 Low-Complexity Lossless and Near-Lossless Multispectral and Hyperspectral Image Compression Standard," 6th International Workshop on On-Board Payload Data Compression (OBPDC), Sep. 20-21, 2018, Matera, Italy.

[3]   *Lossless Multispectral & Hyperspectral Image Compression.* Report Concerning Space Data System Standards, CCSDS 120.2-G-0. Green Book. Issue 1. Washington, D.C.: CCSDS, December 2015.

[4]   M. Klimesh, "Low-complexity lossless compression of hyperspectral imagery via adaptive filtering," *IPN Progress Report*, vol. 42–163, pp. 1–10, Nov. 15, 2005. [Online]. Available: http://ipnpr.jpl.nasa.gov/progress_report/42-163/163H.pdf

[5]   D. Keymeulen et al., "High Performance Space Data Acquisition and Compression with Embedded System-on-Chip Instrument Avionics for Space-based Next Generation Imaging Spectrometers (NGIS)", *Proceedings of 27th Annual Single Event Effects (SEE) Symposium and Military and Aerospace Programmable Logic Devices (MAPLD) Workshop*, May 2018, La Jolla, CA, 2018.

[6]   D. Keymeulen et al., "High Performance Space Data Acquisition, Clouds Screening and Data Compression with modified COTS Embedded System-on-Chip Instrument Avionics for Space-based Next Generation Imaging Spectrometers (NGIS)," 6th International Workshop on On-Board Payload Data Compression (OBPDC), Sep. 20–21, 2018, Matera, Italy.

[7]   S. W. Golomb, "Run-length encodings," *IEEE Transactions on Information Theory*, IT-12(3):399–401, July 1966.

[8]   *Lossless Data Compression.* Recommendation for Space Data System Standards, CCSDS 121.0-B-2. Blue Book. Issue 2. Washington, D.C.: CCSDS, April 2012.

[9]   P. G. Howard, "Interleaving Entropy Codes," in *Proc. Compression and Complexity of Sequences 1997*, pp. 45–55, 1998.

[10]   A. Kiely, M. Klimesh, "A New Entropy Coding Technique for Data Compression," *IPN Progress Report*, vol. 42-146, pp. 1–48, 2001.